Journal of Fluids and Structures (2000) **14,** 403–428
doi:10.1006/jfls.1999.0276, available online at http://www.idealibrary.com on IDEAL®

A NUMERICAL STUDY OF CYLINDERS IN WAVES AND CURRENTS

C. Y. Zhou and J. M. R. Graham

Department of Aeronautics, Imperial College, London SW7 2BY, U.K.

(Received 5 March 1999, and in final form 10 November 1999)

The research on combination flow of planar oscillatory flow plus an in-line steady stream is of importance to the situation of structures in waves and current. The combination flow has not been studied extensively. There is still little information about the effect of current and about combined effect of current and waves on hydrodynamic loading of the structures. The present study investigates the combination flow around a circular cylinder using a vortex-based method incorporating vortex moving particles (discrete vortices) with a finite-difference scheme for the vorticity diffusion. The main attention is paid to the effects of a small current on in-line fluid forces and vortex patterns in the wake. Morison's equation and an equation with two drag terms are examined. The results show that the presence of a small current in an oscillatory flow can reduce the drag coefficient significantly. Morison's equation gives reasonably good predictions for the in-line forces for an oscillatory flow plus a small current. The current tends to bring the whole vortex wake downstream and tries to form the stable Karman asymmetrical form in the downstream wake. The present results show certain agreement with some previous experimental results.

1. INTRODUCTION

Flow around cylinders has been a research topic in fluid mechanics for decades because of its complex physical phenomena, such as separation and vortex shedding, and also its practical importance in many industrial fields. In practice, the problems arise from the interest in predicting loads on structures due to the fluid motion. The study of a two-dimensional oscillatory flow around a cylinder is often practically related to the case of a cylindrical structure in waves. When the vertical velocity component is neglected, the wave flow around a vertical column of a tension leg platform or fixed jacket structure, and the flow around a flexible vertical cylinder such as a riser pipe are strongly similar to a sinusoidally oscillating planar flow about a cylinder. The present research into harmonic oscillatory flow combined with a steady flow past a circular cylinder is of importance to the situation of structures in waves and current.

For a planar oscillatory cross-flow about a circular cylinder, there has been a large number of experimental and numerical studies carried out, which provide the basic knowledge to further understand more complex wave flows such as waves plus currents. It is known that the in-line force F_x on a circular cylinder in an oscillatory flow can be represented by a sum of drag and inertial forces, which is known as Morison's equation (Morison *et al.* 1950),

$$F_x = \tfrac{1}{2}\rho D C_d u(t)|u(t)| + \rho \tfrac{1}{4}\pi D^2 C_m \frac{\mathrm{d}u(t)}{\mathrm{d}t}, \tag{1}$$

where ρ is the density of fluid, D the diameter of the cylinder, $u(t)$ the velocity of flow, and t the time. The drag and inertia coefficients are C_d and C_m which are assumed constant over

0889–9746/00/040403 + 26 $35.00/0

the flow cycle and may be obtained through Fourier analysis. It was shown that C_d and C_m are functions of a parameter $U_w T/D$ (Keulegan & Carpenter 1958), where U_w is the maximum velocity of the oscillation and T is the period of the oscillation. The parameter was later named the Keulegan–Carpenter number KC. The magnitude of KC indicates the relative importance of drag and inertia forces. When KC is smaller than about 5, the cylinder is mainly subject to inertia force. This regime is called the inertia regime. But since the drag force determines the hydrodynamic damping, the drag force may be important in this regime for certain types of problem, even though it is small compared to the inertia force. In the KC range of $5 < \mathrm{KC} < 25$, named the inertia/drag regime, the drag force and inertia force, as the direct forces, are both important. Beyond $\mathrm{KC} > 25$ the drag force becomes dominant, but changes in the inertia force may sometimes be significant in affecting natural frequencies of oscillating systems. This regime is defined as the drag regime.

Another important parameter to describe these flows is defined as $\beta = D^2/\nu T = \mathrm{Re}/\mathrm{KC}$, the Stokes parameter, where Re is the Reynolds number and ν is the kinematic viscosity. Sarpkaya (1986) showed that the inceptions of the Honji instability of azimuthally directed vortices (Honji 1981), separation, and turbulence depend on both KC and β. For a given β value, the oscillatory flow around a circular cylinder at low KC can be classified into four different flow regimes according to how the drag and inertia coefficients change with KC: (i) $\mathrm{KC} < \mathrm{KC}_r$, drag coefficient C_d decreases as KC increases and the inertia coefficient C_m is independent of KC, while the laminar flow is attached, stable and two-dimensional; (ii) $\mathrm{KC}_r < \mathrm{KC} < \mathrm{KC}_{md}$, C_d decreases and reaches its minimum value at KC_{md} where the flow has just separated; in this region, Honji instability, separation and turbulence occur successively, giving rise to increases in the values of the force coefficients; apart from these regions of increase, C_m keeps nearly constant; (iii) $\mathrm{KC}_{md} < \mathrm{KC} < \mathrm{KC}^*$, C_d increases and C_m decreases as KC increases and reach maximum and minimum values, respectively, at KC*; and (iv) $\mathrm{KC} > \mathrm{KC}^*$, C_d decreases and C_m increases as KC increases further.

The magnitude of KC also indicates different flow modes. Several different regimes were illustrated by Williamson (1985) according to how the vortices form, shed, grow and convect. The regimes are: (i) pairing of attached vortices ($0 < \mathrm{KC} < 7$), where for $\mathrm{KC} < 1{\cdot}5$ no separation occurs, for $\mathrm{KC} < 4$ the flow was observed to be symmetrical, and for $4 < \mathrm{KC} < 7$, the vortices were found to be unequal in strength and the vortex pairs did not form simultaneously; (ii) transverse street single pair regime ($7 < \mathrm{KC} < 15$), where one large vortex is shed during each half cycle and a transverse street forms; (iii) double pair regime ($15 < \mathrm{KC} < 24$), where two large vortices are shed in each half-cycle, and two vortex pairs form in each cycle; (iv) three pair regime ($24 < \mathrm{KC} < 32$), where there are predominantly three vortices shed in each half cycle, and four pair regime ($32 < \mathrm{KC} < 40$) where four pairs of vortices form in a full cycle. For larger-amplitude flow, the wake patterns were observed to be irregular and less repetitive. Obasaju *et al.* (1988) using a U-tube also reported that asymmetrical flow began at $\mathrm{KC} \simeq 4$. Bearman *et al.* (1978) observed some near-repetitive vortex patterns. The main vortex patterns above $\mathrm{KC} \simeq 8$ were found to be a "sideways" street (for $8 < \mathrm{KC} < 15$) and a cyclic regime (for $15 < \mathrm{KC} < 25$). Above $\mathrm{KC} \simeq 25$, they found that the wake resembled a limited length Karman street in each half-cycle.

Combined motion of an oscillatory flow $U_w \sin(\varpi t)$, where $\varpi = 2\pi/T$, and a mean stream U_c has also been studied. Conventionally, the in-line force is written as a straightforward expression of Morison's equation (1), where $u(t)$ is now the combined velocity of the mean stream and the oscillation:

$$F_x = \tfrac{1}{2}\rho D C_d U_w^2 (B + \sin(\varpi t))|B + \sin(\varpi t)| + \rho \tfrac{1}{2}\pi D^2 U_w C_m \frac{\partial(\sin(\varpi t))}{\partial t}, \tag{2}$$

where $B = U_c/U_w$. It is known that current has effects on the motion of vortices and the influence of current on wave loading is quite considerable (Sarpkaya & Isaacson 1981). A survey by Sarpkaya & Isaacson (1981) indicated that, for at least relatively small Reynolds numbers and sufficiently small values of B, the drag coefficient as defined by equation (2) for a current-harmonic combination flow may be considerably smaller than that for a harmonic flow alone, i.e. $B = 0$. In an analysis of wave force data, Dalrymple (1975) showed that neglecting current could have serious consequences in over-predicting the drag coefficient in Morison's equation.

From a desire to investigate the damping of vibrations of offshore structures excited by waves and current, Verley & Moe (1979a, b) did considerable analysis and experimental work for a combined flow of a cylinder oscillating in a current. The experimental results were analysed using two equations: Morison's equation (2), and an extended Morison's equation which contained two drag terms, the steady and oscillatory drag terms, and an inertial term

$$F_x = \tfrac{1}{2}\rho D C_{do} U_w^2 \sin(\varpi t))|\sin(\varpi t)| + \tfrac{1}{2}\rho D C_{dc} U_c^2 + \rho \tfrac{1}{4}\pi D^2 U_w C_m \frac{\partial(\sin(\varpi t))}{\partial t}, \tag{3}$$

where C_{do} and C_{dc} are the drag coefficients for oscillatory flow and steady flow. Their results indicate that the current did affect the oscillatory component of force, and neglecting the effect of a current may result in overestimating the oscillatory part of the force and hence the fluid damping. Obasaju *et al.* (1991) have studied a combined flow for β in range of 300–1600 and reduced velocity V_r ($= U_c T/D$) from 0 to 20 with moderate values of KC by oscillating a circular cylinder in-line with a steady current of water. Their results showed that for KC = 10, 14 and 18, significantly lower values of C_d tended to occur when there was a current, but little effect of current was found when KC = 34. Sarpkaya *et al.* (1992) carried out a numerical investigation on a circular cylinder in oscillatory plus steady mean flow using the finite-difference method. Their results have revealed the existence of an interesting wake, comprised of three rows of heterostrophic vortices at certain values of KC and B.

However, the combination motion has not been studied as extensively as planar oscillatory flow. There is still little information about the effect of current and combined effect of current and waves on hydrodynamic loading of the structures. Morison's equation has been known as a good empirical expression for the in-line force for a planar oscillatory stream. For more complex oscillating flows, such as oscillatory flow plus a steady flow, there is a need to examine further whether the equation can still represent the in-line forces with constant coefficients C_d and C_m throughout a given oscillating cycle as well as it does for harmonic oscillatory flow.

With the aim of developing more understanding of the combination motion around a cylinder, a numerical investigation, using a vortex-based method incorporating vortex moving particles (discrete vortices) with a finite-difference scheme for the vorticity diffusion, for combinations of sinusoidally oscillatory flow plus steady flow $u(t) = U_w \sin(\varpi t) + U_c$ past a fixed circular cylinder is carried out in the present work. This, planar flow, is taken to simulate the effect of waves plus a current passing a stationary cylindrical element of a structure. Since the phenomenon of a cylinder oscillating in a current is similar to that of a cylinder subjected to a combination flow of harmonic waves and current, the present investigation might also give some information on the effects of vortex-induced in-line oscillations.

The objective of the present work is to investigate the effects of a small current ($B \leq 1$) on the vortex shedding, vortex patterns, and forces on the cylinder in an oscillatory flow. The extended Morison's equation (2) and equation (3) are examined. In the present calculation,

turbulent effects are not considered and the flow is assumed to be two-dimensional. Therefore, the calculation is limited to low Reynolds numbers. The parameter β is set at 200 for all calculations, and KC varies from 0·2 to 26, i.e. in the inertia and inertia/drag regimes. The current to wave amplitude velocity ratio B covers the range 0–1 in steps of 0·25.

2. THE VORTEX METHOD

The original discrete vortex method was developed for inviscid flow and later, incorporating the random walk, was used for viscous flow (Chorin 1973). The method is based on the theorem that, in an inviscid incompressible fluid, vorticity is a kinematic property of fluid particles. It can neither be created nor destroyed. Vortex lines are material lines and remain continually composed of the same fluid elements. They can only undergo convection and deformation. In a viscous fluid, however, vorticity is generated by the streamwise pressure gradient along a boundary and is subject to diffusion as well as convection and deformation. These processes determine the whole vorticity and hence the velocity field, which in turn controls the production of vorticity.

Chorin (1973) introduced the split-time step approach to solve the Navier–Stokes equations. These equations expressed in vorticity–velocity form, eliminating pressure, are sequentially integrated forward in time, separately for the diffusion and then the convection and deformation. For two-dimensional flows, which were considered by Chorin and will be considered here, deformation (stretching and rotation of vorticity) is identically zero. Hence, the vorticity (ω) transport equation is

$$\frac{\mathrm{D}\omega}{\mathrm{D}t} = \nu\nabla^2\omega; \quad \frac{\mathrm{D}\omega}{\mathrm{D}t} \equiv \frac{\partial\omega}{\partial t} + u\frac{\partial\omega}{\partial x} + v\frac{\partial\omega}{\partial y}. \tag{4}$$

In that case, one part of the split-time step evaluates the change in vorticity ω given by

$$\frac{\partial\omega}{\partial t} = \nu\nabla^2\omega, \tag{5}$$

and the other part, the convection equation,

$$\frac{\partial\omega}{\partial t} + u\frac{\partial\omega}{\partial x} + v\frac{\partial\omega}{\partial y} = 0 \qquad \left(\text{or } \frac{\mathrm{D}\omega}{\mathrm{D}t} = 0\right). \tag{6}$$

Inviscid flow only requires equation (6) to be solved for the transport of vortcity. This is performed by moving vortex particles (discrete vortices) which conserve their circulation with the local velocity field. In Chorin's split-time slip method, equation (5) was satisfied for viscous flow in a grid-free manner by the random walk simulation of this equation. This method has some disadvantages relating to its slow convergence with increasing number of vortices and the fact that the diffusion coefficient (ν) must be constant or of restricted variability. Other grid-free methods solve the diffusion equation by computing its Green's function over interacting vortex "blobs" [see Koumoutsakos *et al.* (1994)].

The method used in the present work takes an alternative approach. The diffusion step and also the velocity field as in a conventional Eulerian flux method are solved on a fixed mesh (by a finite-difference method in the present code). However, the convection substep continues to be solved by a Lagrangian moving-particle method involving discrete vortices. This hybrid method (Graham 1988) retains some of the advantages of both methods but requires projection of vorticity and velocity between the two systems (mesh and particles).

Two-dimensional viscous flow of an incompressible fluid can be described by the transport equation (4) for the vorticity ω and a Poisson equation relating the stream

function ψ (i.e., the velocity field) to the vorticity field,

$$\nabla^2\psi = -\omega. \tag{7}$$

To calculate the combined flow past the circular cylinder, a polar mesh (r, θ) is used, where the boundary of the mesh at the wall coincides with the cylinder surface. Since in the boundary layer every quantity changes rapidly in the radial direction, it is convenient to use a mesh that has more grid points near the surface in the radial direction than far from the surface. A conformal transformation, $z = Re^{-i\alpha\zeta}$, is used to transform $z(x, y)$ the physical polar mesh into a Cartesian computational mesh $\zeta(\xi, \eta)$, where R is the radius of the circular cylinder, $\alpha = 2\pi/l$ and l is the length of the computational domain in the ξ direction. This transformation takes the circle to the straight line $0 \leq \xi \leq l$, $\eta = 0$. With this transformation, a regular Cartesian mesh in the computational plane becomes a polar mesh which is uniform in the circumferential direction and expands exponentially in the radial direction. This satisfies the need for a greater density of mesh points near the cylinder surface in the physical plane. In the computational plane, equations (4) and (7) become

$$J\frac{\partial\omega}{\partial t} + \frac{\partial\psi}{\partial\eta}\frac{\partial\omega}{\partial\xi} - \frac{\partial\psi}{\partial\xi}\frac{\partial\omega}{\partial\eta} = \nu\left(\frac{\partial^2\omega}{\partial\xi^2} + \frac{\partial^2\omega}{\partial\eta^2}\right), \tag{8}$$

$$\frac{\partial^2\psi}{\partial\xi^2} + \frac{\partial^2\psi}{\partial\eta^2} = -J\omega, \tag{9}$$

where $J = (R\alpha e^{\alpha\eta})^2$ is the Jacobian of the transformation.

Applying the splitting operator (Chorin 1973), equation (8) is written as a convection part and a diffusion part:

$$\left[\frac{\partial\omega}{\partial t}\right]_1 = \frac{1}{J}\left(\frac{\partial\psi}{\partial\xi}\frac{\partial\omega}{\partial\eta} - \frac{\partial\psi}{\partial\eta}\frac{\partial\omega}{\partial\xi}\right), \tag{10}$$

$$\left[\frac{\partial\omega}{\partial t}\right]_2 = \frac{1}{J}\left(\nu\left(\frac{\partial^2\omega}{\partial\xi^2} + \frac{\partial^2\omega}{\partial\eta^2}\right)\right), \tag{11}$$

with

$$\frac{\partial\omega}{\partial t} = \left[\frac{\partial\omega}{\partial t}\right]_1 + \left[\frac{\partial\omega}{\partial t}\right]_2.$$

The two parts are solved sequentially. In the discrete vortex method, the vorticity field is represented by a large set of discrete point vortices carrying circulation Γ_k, $k = 1, 2, \ldots, N_{\bar{v}}$. Equation (10) is satisfied by moving these vortex particles of constant circulation at the velocity in the computation plane but modified by the Jacobian. The velocity field for this is obtained by solving equation (9) on the mesh where the right-hand side of equation (9), i.e., the vorticity values on the mesh points, is evaluated from the circulation Γ_k carried by the vortex particles. The following area-weighted projection scheme achieves this on the Cartesian mesh shown in Figure 1, conserving circulation and its first moments:

$$\omega_m = \frac{\Gamma_k A_m}{A^2}, \quad m = 1, 2, 3, 4, \tag{12}$$

where Γ_k is the circulation of the kth vortex and A is the area of the mesh cell.

Based on this vorticity field, equation (9) is solved by first using Fourier transformation with respect to ξ, since the flow field is periodic in that direction:

$$\bar{\psi} = \int \psi e^{-ik\xi}\, d\xi.$$

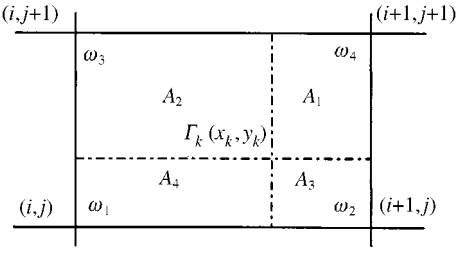

Figure 1. The area-weighted projection scheme.

Applying this transformation to equation (9) gives

$$-k^2\bar{\psi} + \bar{\psi}_{\eta\eta} = -\overline{J\omega}, \tag{13}$$

where $\overline{J\omega}$ is the Fourier transform of $J\omega$. On the body surface, the boundary condition $\psi = 0$ is applied. On the far-field boundary, ψ is determined by Biot–Savart integration from the vorticity on the grid including the effect of image vorticity in the body compatible with the $\psi = 0$ boundary condition. The calculation of the more exact boundary condition on the outer boundary is computationally expensive, and only every eighth grid point is evaluated by this integration, while the rest are determined by interpolation. However, it is found to improve the solution. After the values of ψ at the mesh grids have been obtained, the velocity components on the mesh points are then calculated by applying a central differencing scheme:

$$u = \frac{\partial\psi}{\partial\xi}, \qquad v = -\frac{\partial\psi}{\partial\eta}.$$

The velocity field is then projected onto the vortex particles for convection using the same area-weighting interpolation scheme:

$$u_k = \frac{u_m A_m}{A}, \qquad v_k = \frac{v_m A_m}{A}, \qquad m = 1, 2, 3, 4.$$

The point vortices at (ξ_k^n, η_k^n), $k = 1, 2, \ldots, N_v$, are convected to their new positions $(\xi_k^{n+1}, \eta_k^{n+1})$ using first-order time integration,

$$\xi_k^{n+1} = \xi_k^n + \frac{1}{J} u_k \Delta t \quad \text{and} \quad \eta_k^{n+1} = \eta_k^n + \frac{1}{J} v_k \Delta t.$$

Up to this point, the method is the same as the inviscid vortex-in-cell method [see, e.g., Christiansen (1973)]. In the present work an explicit finite difference scheme is used to solve the diffusion equation (11). An outer boundary condition $\omega = 0$ has been used here. The calculation is stopped before any vorticity of significant size reaches the outer boundary consistent with this boundary condition. Other boundary conditions are easily applied and would have been necessary for higher Keulegan–Carpenter numbers than were studied on this mesh. This condition was not restrictive for the flows being examined. At the body surface, the value of vorticity is determined from the stream function and the value of vorticity at the first mesh point off the surface by a second-order Taylor series satisfying the no-slip boundary condition at the wall. The change in vorticity due to diffusion, obtained by solving equation (11) at each grid point, is projected back onto the point vortices using the same area-weighted projection, creating new vortices at grid points where necessary. This process conserves the total circulation and its first moments and also has the advantage that

numerical diffusion never becomes comparable with the molecular diffusion, even if v is very small.

Having obtained the diffused vorticity field over the time step, equation (10) is solved again to give the new velocity field. Finally, the point vortices are convected by this velocity field to new positions using a first-order method. Higher-order time integration is possible but was not found necessary here, as the time steps used were small for stability reasons. This time step is repeated as often as required.

3. FORCE CALCULATIONS

For a cylinder immersed in a time-dependent inviscid flow $u(t)$, the drag and lift forces (F_x, F_y) may be derived from the momentum theorem including the potential flow inertia term and a term for the vortices in the flow field and their images in the cylinder:

$$F_x(t) + \mathrm{i}F_y(t) = \frac{1}{4}\pi\rho C_{\mathrm{m}0} D^2 \frac{\partial u(t)}{\partial t} - \mathrm{i}\rho \frac{\partial}{\partial t} \sum_{k=1}^{N_v} \Gamma_k \left(Z_k - \frac{R^2}{Z_k^*} \right), \tag{14}$$

where C_{m0} is the inertia coefficient, equal to 2·0 for a circular cylinder; Z_k is the complex coordinate, $x_k + \mathrm{i}y_k$, of the kth vortex; and Z_k^* is the conjugate of Z_k.

Equation (14) has been shown by Wu (1981) to be applicable to viscous flow. It can be difficult to use in experiments since it requires the information of the position and strengths of the whole vorticity field at subsequent times. However, it is convenient to apply in a numerical calculation, especially when using a vortex method. In the present work, the sum is calculated from the vorticity on the grid points, rather than from the much larger number of point vortices in the flow field in order to reduce the amount of calculation.

Another way to calculate the forces is to find the pressure and shear stress distributions on the surface. It is convenient to use a relationship between the vorticity and the pressure p at the wall,

$$\left.\frac{\partial p}{\partial s}\right|_w = -\mu \left.\frac{\partial \omega}{\partial r}\right|_w,$$

derived from the Navier–Stokes equation with the non-slip condition at the wall, where s is the curvilinear coordinate along the surface and μ is the viscosity of fluid. Then the pressure on the surface is obtained from

$$p_j = p_{\mathrm{ref}} - \mu \int_{s_{\mathrm{ref}}}^{s_j} \left.\frac{\partial \omega}{\partial r}\right|_w \mathrm{d}s,$$

where p_{ref} is a reference pressure and may be the pressure value at front stagnation point. Strictly, p_{ref} should be calculated by integrating from far upstream but, since the choice of p_{ref} does not affect the forces, it is often convenient to assume that the stagnation pressure coefficient equals to unity, although this is only approximately true. The contribution from the shear stress is $\tau = -\mu\omega|_w$. Therefore, the total force F is obtained by the following integral on the surface:

$$F = F_x + \mathrm{i}F_y = -\sum_{j=1}^{n} [p_j - \mathrm{i}\mu(\omega_j)_w] \mathrm{e}^{\mathrm{i}\theta_j} \Delta s_j, \tag{15}$$

where i denotes the unit complex number and j indicates the jth grid point on the wall.

The main drawback of this method is that, since p is related to the normal gradient of vorticity at the body surface, the resulting force is very noisy. A better but more

computationally expensive method solves a Poisson equation for p with Neumann boundary conditions on the body.

4. EVALUATION OF FORCE COEFFICIENTS

The two forms of in-line force expressions from Morison's equation (2) and equation (3) have been used to analyse the calculated force time histories. For equation (2) there are two extreme cases. One is $B \to \infty$, i.e. $V_r \gg \mathrm{KC}$, for which the drag term should reduce to the form for steady flow, and the inertia term vanishes. The other one is $B \to 0$, i.e. $V_r \ll \mathrm{KC}$, for which equation (2) reduces to equation (1) for a planar oscillatory flow. It is expected that, when $B \to \infty$, C_d in equation (2) and C_{dc} in equation (3) tend to the same value as for a steady flow; and, when $B \to 0$, C_d and C_{do} tend to the value for a planar oscillatory flow.

For a planar oscillatory flow, the force coefficients in equation (1) are assumed to be constant through the cycle and usually determined using Fourier averaging (Keulegan & Carpenter 1958). For a combined flow of a planar oscillatory flow and a steady current, the in-line force may be divided into a mean part $\bar{F}_x$ and an oscillating part $F'_x(t)$ (see Figure 2):

$$F_x(t) = \bar{F} + F'_x(t), \quad \text{where } \bar{F}_x = \frac{1}{T}\int_0^T F_x(t)\,\mathrm{d}t \quad \text{and } \frac{1}{T}\int_0^T F'_x(t)\,\mathrm{d}t = 0.$$

In equation (2) the steady drag and oscillatory drag forces are mutually dependent which makes the determination of the drag force coefficient more complex. In the present work, it is attempted to determine the drag coefficient both from the oscillatory part of the force and the mean part of the force. This gives two drag coefficient values for equation (2), and in general these two drag coefficient values are not equal. In such a way, the effect of a small current on the force coefficients is then investigated by comparing these drag coefficient values with those for the planar oscillatory flow. The drag coefficient evaluated from the oscillatory part of the force is referred to here as the oscillatory drag (coefficient C_{d1}) and from the mean part of the force referred to here as the steady drag (coefficient C_{d2}).

Let

$$g(t) = (B + \sin(\varpi t))|B + \sin(\varpi t)| \quad \text{and} \quad g'(t) = g(t) - \overline{g(t)},$$

where

$$\overline{g(t)} = \frac{1}{T}\int_0^T g(t)\,\mathrm{d}t = \frac{1}{\pi}[(2B^2 + 1)\sin^{-1}(B) + 3B\sqrt{(1 - B^2)}],$$

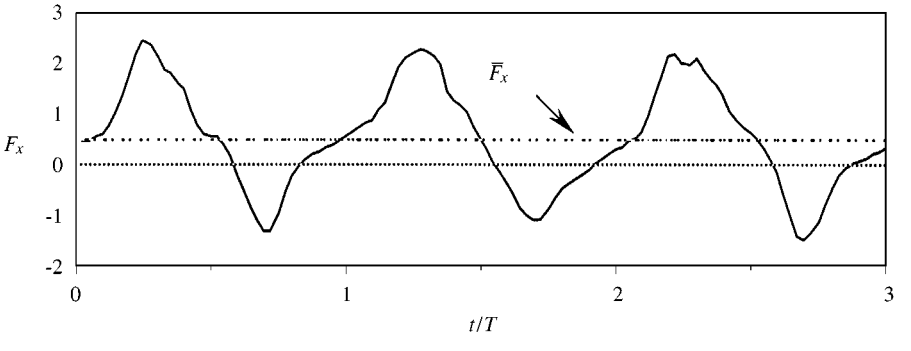

Figure 2. The in-line force on a cylinder in waves and a current.

with $\overline{g(t)} = 0$ when $B = 0$. Writing equation (2) in terms of an oscillatory component and a mean component of force, and using C_{d1} and C_{d2}, we have

$$F_x'(t) = \frac{1}{2}\rho D U_w^2 C_{d1} g'(t) + \rho \frac{1}{4}\pi D^2 U_w C_m \frac{\partial}{\partial t}(B + \sin(\varpi t)) \quad \text{and}$$

$$\overline{F_x(t)} = \frac{1}{2}\rho D U_w^2 C_{d2} \overline{g(t)}. \tag{16a,b}$$

The values of C_{d1} and C_{d2} are then determined by the following formulae:

$$C_{d1} = \frac{1}{b_1}\left(\frac{2}{T}\int_0^T \frac{F_x(t)\sin(\varpi t)}{\frac{1}{2}\rho D U_w^2}\,\mathrm{d}t\right) \quad \text{and} \quad C_{d2} = \frac{1}{\overline{g(t)}}\frac{\overline{F_x(t)}}{\frac{1}{2}\rho D U_w^2}, \tag{17a,b}$$

where

$$b_1 = \frac{1}{\pi}\left(\tfrac{4}{3}B^2\sqrt{(1-B^2)} + 4B\sin^{-1}(B) + \tfrac{8}{3}\sqrt{(1-B^2)}\right), \tag{18}$$

and $b_1 = 8/3\pi$ when $B = 0$.

In equation (3) the steady and oscillatory drag forces are independent. The determination of the drag coefficients is relatively simple as the oscillatory part and the mean part are directly related to the oscillation velocity and the steady flow velocity. The formulae are

$$C_{do} = \frac{3\pi}{8}\left(\frac{2}{T}\int_0^T \frac{F_x \sin(\varpi t)}{\frac{1}{2}\rho U_w^2 D}\,\mathrm{d}t\right) \quad \text{and} \quad C_{dc} = \frac{\overline{F_x(t)}}{\frac{1}{2}\rho D U_c^2}. \tag{19a,b}$$

When $B = 0$, $C_{do} = C_{d1}$ and $C_{dc} = 0$. The inertia coefficient C_m in both equations (2) and (3) is determined by

$$C_m = \frac{KC}{\pi^2}\left(\frac{2}{T}\int_0^T \frac{F_x \cos(\varpi t)}{\frac{1}{2}\rho U_w^2 D}\,\mathrm{d}t\right). \tag{20}$$

The hydrodynamic damping C_{dmp} is given by the drag forces in phase with the oscillatory velocity and can be calculated by the following formula (Verley & Moe, 1979b):

$$C_{dmp} = \frac{\int_0^T F_x(t) U_w \sin(\varpi t)\,\mathrm{d}t}{\int_0^T U_w^2 \sin^2(\varpi t)\,\mathrm{d}t} = \frac{2}{U_w T}\int_0^T F_x(t)\sin(\varpi t)\,\mathrm{d}t.$$

Given the force $F_x(t)$ from equations (2) and (3), C_{dmp} has the following relationships with C_{d1} and C_{do}:

$$C_{dmp} = \tfrac{1}{2}\rho D U_w b_1 C_{d1}, \tag{21}$$

$$C_{dmp} = \frac{4\rho D U_w}{3\pi} C_{do}. \tag{22}$$

5. VALIDATION TEST

In order to examine the implementation of the numerical model on a computer and the reliability of the computer code, a set of initial tests in steady flow at low Re and in a planar oscillatory flow at low KC numbers were carried out. Those values of Re and KC were selected at which the flows are well documented either by experiments or by theoretical

solution so that comparison may be made. For the steady flow, Re = 100 is selected. For the oscillatory flow, KC = 0·2, 0·5, 1·0 and 2·0 with $\beta = 200$ are chosen. Drag and inertia coefficients, Strouhal number St ($= f_s D/U_c$, where f_s is the vortex shedding frequency), force time history and vortex patterns are examined for the purpose. The force on the body is calculated both using the momentum theorem and by calculating the surface pressure and skin friction from the body surface vorticity and its normal gradient as discussed above.

A large number of preliminary calculations were first carried out to determine the optimum values of time step and mesh size for both mean and oscillatory flow cases. It was found that the force obtained by calculating surface pressure and skin friction is quite sensitive to the mesh size, especially to the size of the cells near the wall. This is because the surface pressure is calculated from values on the two mesh grids next to the wall. In contrast, the result from the momentum theorem appears to be much less sensitive to the change of the cell size near the wall. A typical mesh 128×128 ($r \times \theta$) which has typically more than 20 points lying in the boundary layer is used for the steady flow. The preliminary calculations indicate that a value of $\Delta(tU_c/D) = 0{\cdot}00125$ is small enough for both force calculations to produce satisfactory agreement in the results under the selected mesh size. For the oscillatory flow, a mesh 80×128 is used and $\Delta(tU_c/D)$ was varied from 0·001 and 0·0001.

The vortex pattern for Re = 100 (with no oscillatory motion) at time $\Delta(tU_c/D) = 50$ is shown in Figure 3. The figure shows a vortex wake composed of staggered negative and positive vortices, i.e. the well-known von Karman vortex street. The values of St and C_d calculated using the two methods of computing force are compared in Table 1 with some previous experimental data and computational results of other investigators. The result from the momentum theorem yields very good agreement with experimental data and some of the previous computational results. However, the value of the drag coefficient obtained from surface pressure and skin friction calculations is higher than both the experimental data and the main computational results. The lift force is similarly somewhat above accepted computational values. Figure 4 shows the drag and lift time histories where the solid lines are from the momentum theorem and the dashed lines from pressure and skin friction calculations.

The results of the drag and inertia coefficients for a cylinder in an oscillatory flow with $\beta = 200$ are illustrated in Figure 5, together with the theoretical result by Wang (1968), the experimental data of Bearman *et al.* (1985) and Justesen (1991) for $\beta = 196$. It is shown that, as KC increases, the calculated drag coefficient follows the theoretical line well when KC is less than about 2, drops down to a minimum value at about KC = 3, and then increases as KC increases. The calculated inertia coefficient shows approximate independence of KC when KC is less than about 2 in agreement with the theory and then decreases rapidly for KC ≥ 2. The force calculations from both the momentum theorem and the surface pressure and skin friction give close results and are generally in good agreement with the theory and experimental data for KC < 10.

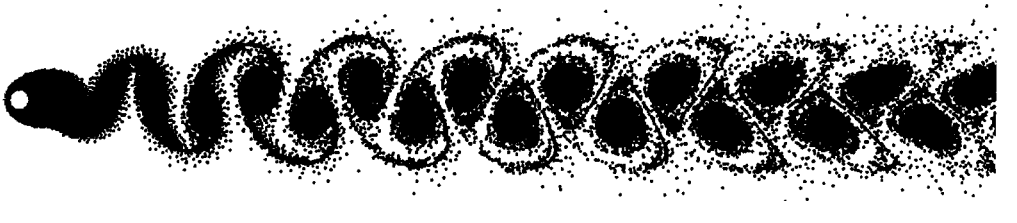

Figure 3. Vortex pattern in the wake, Re = 100, $tU_c/D = 100$.

TABLE 1

Steady flow past a circular cylinder at Re = 100

Investigators	St	C_d	$C_{l\text{rms}}$
Experiments			
Lienhard (experiment, Chaplin *et al.* 1992)	0·155–0·173	1·35–1·49	—
Computations			
Arkell & Graham* (discrete vortex)	—	1·33	0·17
Beaudan & Moin* (high-order finite difference)	—	1·35	0·24
Chaplin (finite difference, Chaplin *et al.* 1992)	0·152	1·82	0·20
Chaplin* (spectral difference)	—	1·29	0·20
Gushchin* (finite difference)	—	1·38	—
Karniadakis* (spectral-element)	—	1·42	0·26
Kravchenko* (Galerkin B-spline)	—	—	0·23
Mittal* (spectral method)	—	—	0·23
Savvides* (spectral difference)	—	1·30	0·16
Savvides* (spectral element)	—	1·32	0·14
Sherwin* (spectral element)	—	1·36	0·24
Stansby (random vortex, Chaplin *et al.* 1992)	0·169	1·36	—
Younis* (finite difference)	—	1·46	0·34
Younis (finite difference, Chaplin *et al.* 1992)	0·168/0·174	1·43/1·45	—
Present result (momentum theorem, discrete vortex)	0·162	1·37	0·20
Present result (surface pressure and skin friction)	0·162	1·48	0·22

* Bearman (1998).

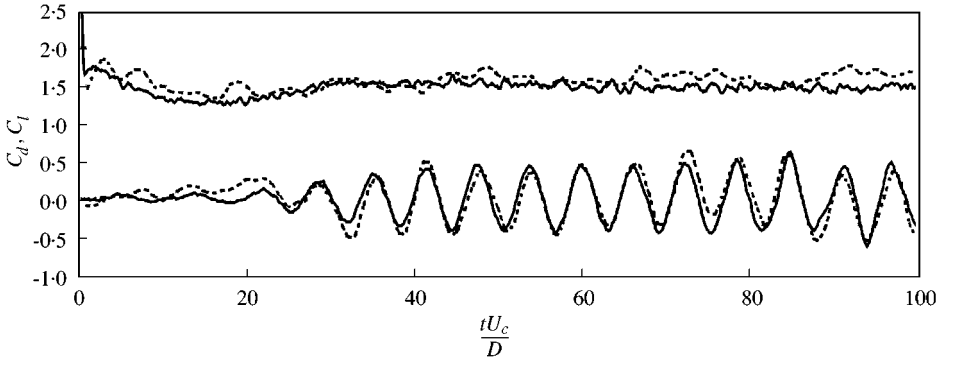

Figure 4. The drag and lift coefficient time histories for Re = 100. Solid line: momentum theorem; dashed line: pressure and skin friction.

Above KC = 10, the calculated C_d is somewhat lower and the C_m is higher than the experimental data. It is thought that this may be due to the fact that the mesh system used is still not fine enough, since it was found that the calculations for higher KC need a very fine mesh to get satisfactory results (Zhou 1994). However, recent computations by Lin *et al.* (1996) show similar departure from the experimental data when a very fine mesh is used. The departure may be due to three dimensionality developing in the flow. For planar oscillatory flow past a circular cylinder with $\beta = 196$, the Honji instability begins at KC $\approx 1{\cdot}63$. At KC > 3 the boundary layer separates and will retain some of this strong three dimensionality which the present two-dimensional laminar code cannot capture, well into the higher KC regime.

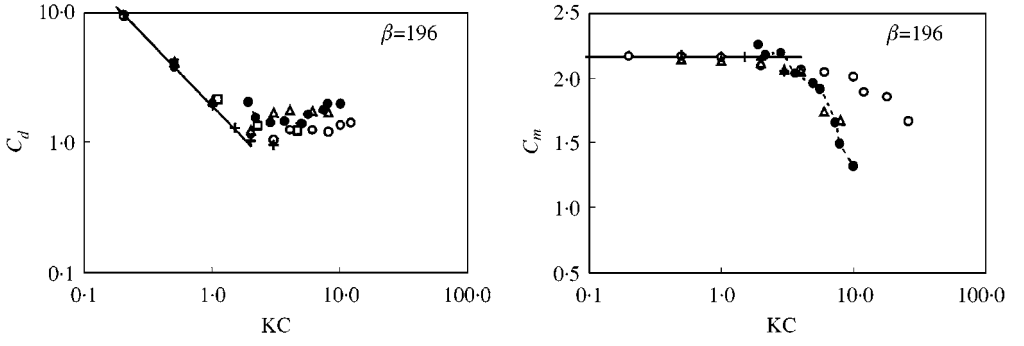

Figure 5. (a) Variation of C_d with KC and (b) variation of C_m with KC for planar oscillatory flow, for the present results $\beta = 200$: ——, theory (Wang 1968); --●--, experiments (Bearman *et al.* 1985); □, computation (Graham & Djahansouzi 1989); +, computation (Justesen 1991); ○, present results (momentum theorem); △, present results (pressure and skin friction).

In the above, the results for force calculated by the momentum theorem appear to be the more independent of the mesh size and time step. Therefore, all of the force calculations in the rest of the work use the momentum theory.

6. EFFECTS OF CURRENT

In order to study the effects of a small current, the combination of sinusoidally oscillatory flow plus steady flow with $B \leq 1$ is investigated. The details of the flow cases are listed in Table 2. The calculated in-line forces are analysed assuming each of the forms of Morison's equation as given in two equations (2) and (3). At present, we are not aware of any data set of low Reynolds numbers to which we can make direct comparisons for validation. However, we feel that the present results exhibit many features of the combined flow and is therefore worth presenting. Attention is drawn to (i) the effects of small current on force coefficients, (ii) the comparison between equations (2) and (3), and (iii) the changes in the vortex pattern due to the small current.

6.1. Force Coefficients

The results versus KC of the force coefficients C_{d1}, C_{d2}, C_{do}, C_{dc} and C_m are presented in Figure 6(a–e) for various velocity ratios. For the version of Morison's equation (2), the value of C_{d1} is seen to decrease as B increases in the range of KC ≥ 2 approximately [see Figure 6(a)] and appears to decrease regularly when KC is smaller than about 1. However, this latter behaviour results from the definition of C_{d1}. It is obvious that

Table 2

Flow cases covered by the present work

B	KC	V_r	Re
0·25	0·2–26	0·05–6·5	10–1300
0·50	0·2–26	0·10–13	20–2600
0·75	0·2–26	0·15–19·5	30–3900
1·00	0·2–26	0·20–26	40–5200

multiplying C_{d1} by $3\pi b_1/8$ should collapse C_{d1} onto the same values as C_{do} [refer to equations (17a), (18) and (18a)] and this turns out to be the case [see Figure 6(c)]. The value of C_{d2} is also seen to decrease as B increases [see Figure 6(b)]. B ot h the values of C_{d1} and C_{d2} are seen to be lower than the drag coefficient value for the planar oscillatory flow alone. It is evident that, if a single drag coefficient value equal to the one for the planar oscillatory flow alone is used in equation (2), the drag force of the combined flow of oscillatory flow and a steady current would be overpredicted. This has clearly shown that the presence of the current is to reduce the drag coefficient C_d in equation (2) for the cases covered in this study.

For the version of Morison's equation with two drag coefficients, i.e., equation (3), the results show that the presence of a current has a significant effect on C_{do} and C_m only when KC is larger than about 2 [see Figure 6(c,e)]. The current appears to increase C_{do} and decrease C_m. The amount of the influence in C_{do} and C_m increases as B. When the current is very small, e.g. B = 0·25, the value of C_{do} is seen to be quite close to the value for the planar oscillatory flow. This is consistent with the findings in the investigation of Verley & Moe (1979b). When KC is smaller than about 1, the value of C_{do} for a wider range of B appears to be very little changed from the value of drag coefficient for the planar oscillatory flow in the Stokes regime. Thus, the current has very little influence on C_{do} in this regime. Similarly, C_m is also not very greatly affected by the presence of the current in this regime. Since C_{do} represents the fluid damping [see formula (22)], Figure 6(c) has shown that the presence of the current does not influence fluid damping very much when the oscillation KC is less than about 1 and increases the fluid damping as B increases when KC is larger than about 2. The drag coefficient C_{dc} from the mean part of the force decreases as B increases [Figure 6(d)].

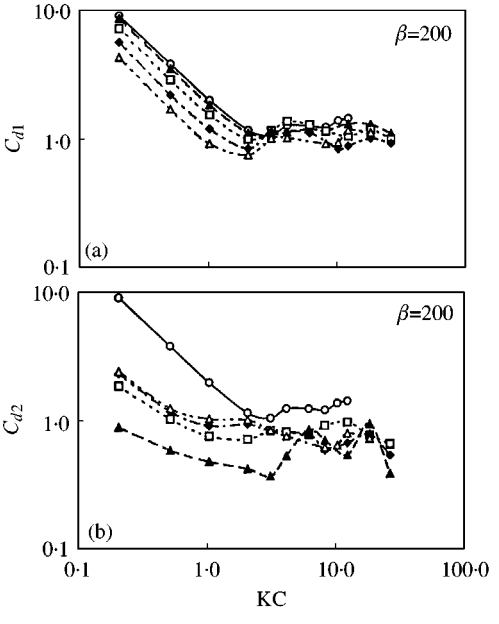

Figure 6. Variation of (a) C_{d1}: —○—, B = 0·00; --▲--, B = 0·25; ---□---, B = 0·50; --◆--, B = 0·75; --△--, B = 1·00, (b) C_{d2}, (c) C_{do}, (d) C_{dc} and (e) C_m with KC for a circular cylinder.
Note: in (b) and (c), —○—, denotes C_{d1} with B = 0·00.

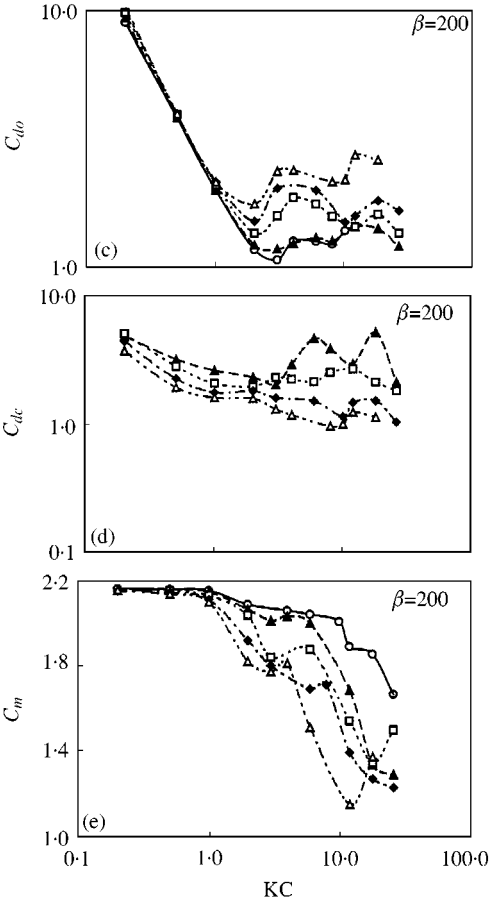

Figure 6. (*Continued*).

In the moderate range of KC ($8 < \mathrm{KC} < 34$), it is known that the presence of a current reduces the drag coefficient C_d in equation (2) and increases the inertia coefficient. This has been shown by some previous studies, e.g. the experimental work presented by Obasaju *et al.* (1991), in which it was found that lower values of C_d tended to occur for $\mathrm{KC} = 10$, 14 and 18 when there was a current. The reduced velocity $U_c T/D$ was in the range from 0 to 20 in the experiment. When $\mathrm{KC} = 34$, the value of C_d was found to be nearly independent of the reduced velocity and close to the value for planar oscillatory flow. In a still higher range of KC, it is reported that the presence of current has little effect on the coefficients (Sarpkaya & Storm 1985).

It is found from the study of planar oscillatory flow (without mean current) that vortex formation tends to cause an increase in drag coefficient C_d and a decrease in C_m. A maximum in C_d and minimum in C_m around $\mathrm{KC} = 15$ is associated with a large vortex formed behind the cylinder (Sarpkaya & Isaacson 1981). It is seen in Figure 6(c) and 6(e) that the variations in oscillatory drag coefficients due to current are strongly and inversely correlated to the variations in inertia coefficient and differ from their values for the planar oscillatory flow (when $\mathrm{KC} \geq 2$). Where C_{do} exhibits an increase, C_m exhibits a reduction. This suggests that the effects are caused by changes in the formation and shedding of the

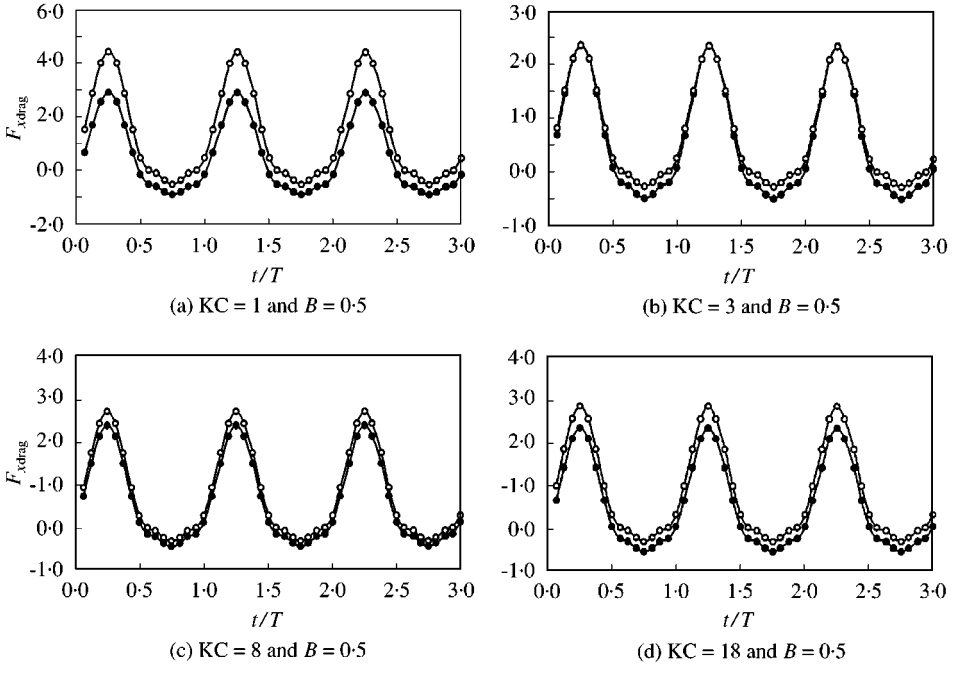

Figure 7. Comparison of drag forces: –●–●–, equation (2) with C_{d1} and C_{d2}; –○–○–, equation (2) with C_d values for planar oscillatory flow.

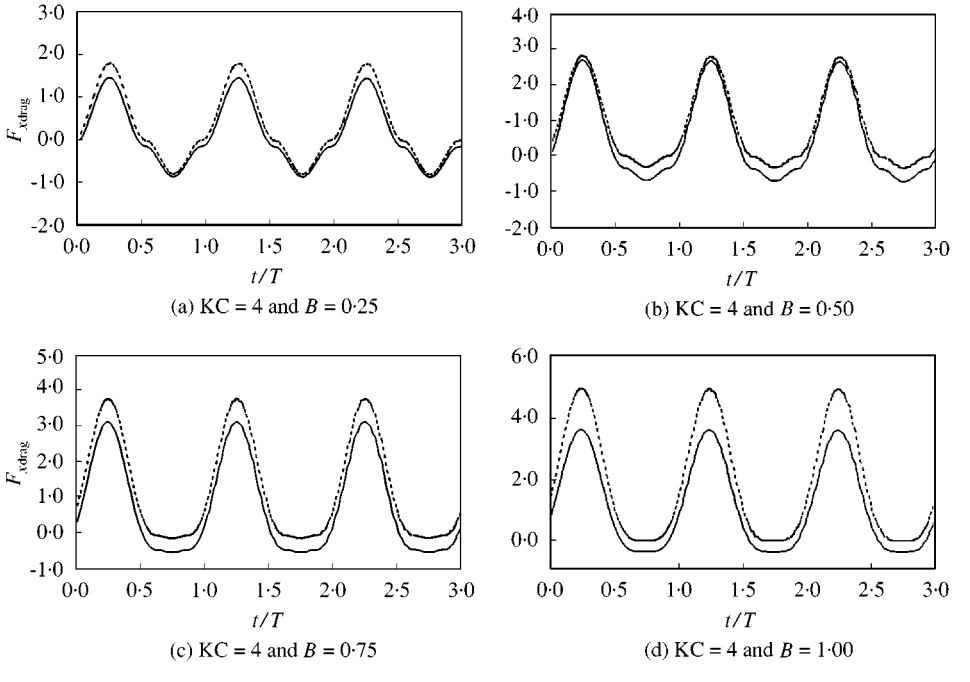

Figure 8. Comparison of drag forces: ——, equation (2) with C_{d1} and C_{d2}; – – –, equation (2) with C_d values for planar oscillatory flow.

vortices with the increasing presence of mean current. The changes in vortex pattern due to current will be discussed in Section 8.

In reality, wave-induced flows in the ocean are often coupled with small currents. The above investigation suggests that calculations which ignore the effect of the current and use the value of C_d of planar oscillatory flow in equation (2) and hence equation (21) for the damping f orce for the combined flow can overpredict the drag and the damping forces. This agrees with the observation on the effect of current made by Sapakaya & Isaacson (1981). This is evident as shown in Figures 7 and 8 where a group of results of drag force F_{xdrag} calculated from equation (2) using C_{d1} for $B = 0{\cdot}0$, and C_{d1} & C_{d2} for different values of B are illustrated. Figure 7 shows the results for KC = 1, 3, 8 and 18 with a fixed value of ($B = 0{\cdot}5$), while Figure 8 is for KC = 4 with B varying from 0·25 to 1 in steps of 0·25. It is seen that the results obtained by using C_{d1} ($B = 0{\cdot}0$), the drag coefficient for oscillatory flow alone, give significantly larger amplitudes of the drag forces, always larger than the results obtained by using the C_{d1} and C_{d2}.

6.2. The Value of KC_{md}

The minimum value of the oscillatory drag coefficient usually occurs at or near the onset of separation for a circular cylinder in planar oscillatory flow (Sarpkaya 1986). The value of Keulegan–Carpenter number KC_{md} at which this minimum value of the oscillatory drag coefficients C_{d1} (or C_{do}) occur (KC $\approx$ 2) is not seen to be significantly affected by the presence of current in the present results [see Figure 6(a,c)]. This suggests that in the case of the combination motion of small current and small oscillations past a circular cylinder this minimum value of the oscillatory drag coefficients does not occur at or near the onset of separation as it does for the planar oscillatory flow because the current alone produces separation. This is supported by further investigations on vorticity fields. One of the results from these investigations is shown in Figure 9(a) for KC = 0·5 and $B = 1{\cdot}0$ (Re = 100). At this KC value, for planar oscillatory flow alone, the flow is still attached while in a steady current at this value of Re a von Karman vortex street is formed. It is found that for the combination motion there is a long period after the start up of the flow during which the numerical solution continues to produce first attached flow and a symmetric wake but eventually separation and an asymmetrical wake with vortex shedding develops.

Regular vortex shedding is predicted [see Figure 9(a)], and the in-line force is seen to be as regular as for the planar oscillatory flow [see Figure 9(b)]. The oscillatory drag and inertia coefficients appear to take almost the same values as for the planar oscillatory flow [see Figure 6(c,e)]. The amplitude of lift force appears to be increased to about twice the value for the steady current case at Re = 100 [see Figure 9(c)]. In this result, the frequency of oscillation is the much higher component (about 12·5 times higher), compared to the frequency of vortex shedding. There is little possibility that a synchronization can occur in this situation. The lift force is still much smaller than the in-line force [see Figure 9(b)] and is therefore less important.

7. MORISON'S EQUATION

7.1. Comparison Between Equations (2) and (3)

Comparisons between calculated and reconstructed force histories from equations (2) and (3), together with the differences between the reconstructed forces and the calculated force, are given in Figure 10(a–d) for KC = 1, 3, 8, and 18 respectively where $B = 0{\cdot}5$. The reconstructed forces from the two equations are both seen to be very close to the computed

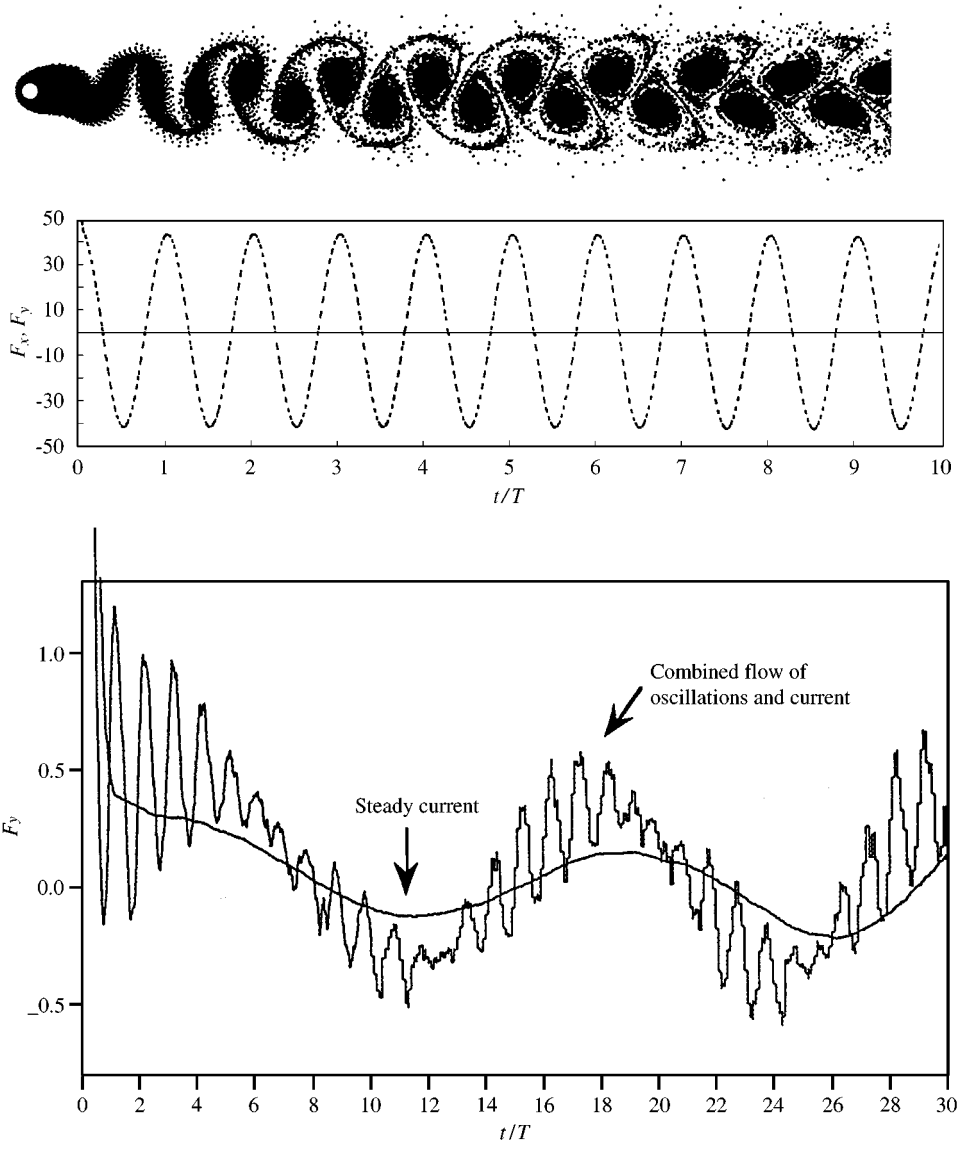

Figure 9. (a) Vortex pattern in the wake, KC = 0·5 and Re = 100. (b) Drag and lift force time histories, KC = 0·5 and Re = 100: ——, F_y; ----, F_x. (c) Lift force time histories of steady current with Re = 100 and combined flow with KC = 0·5 and Re = 100 (B = 1·0).

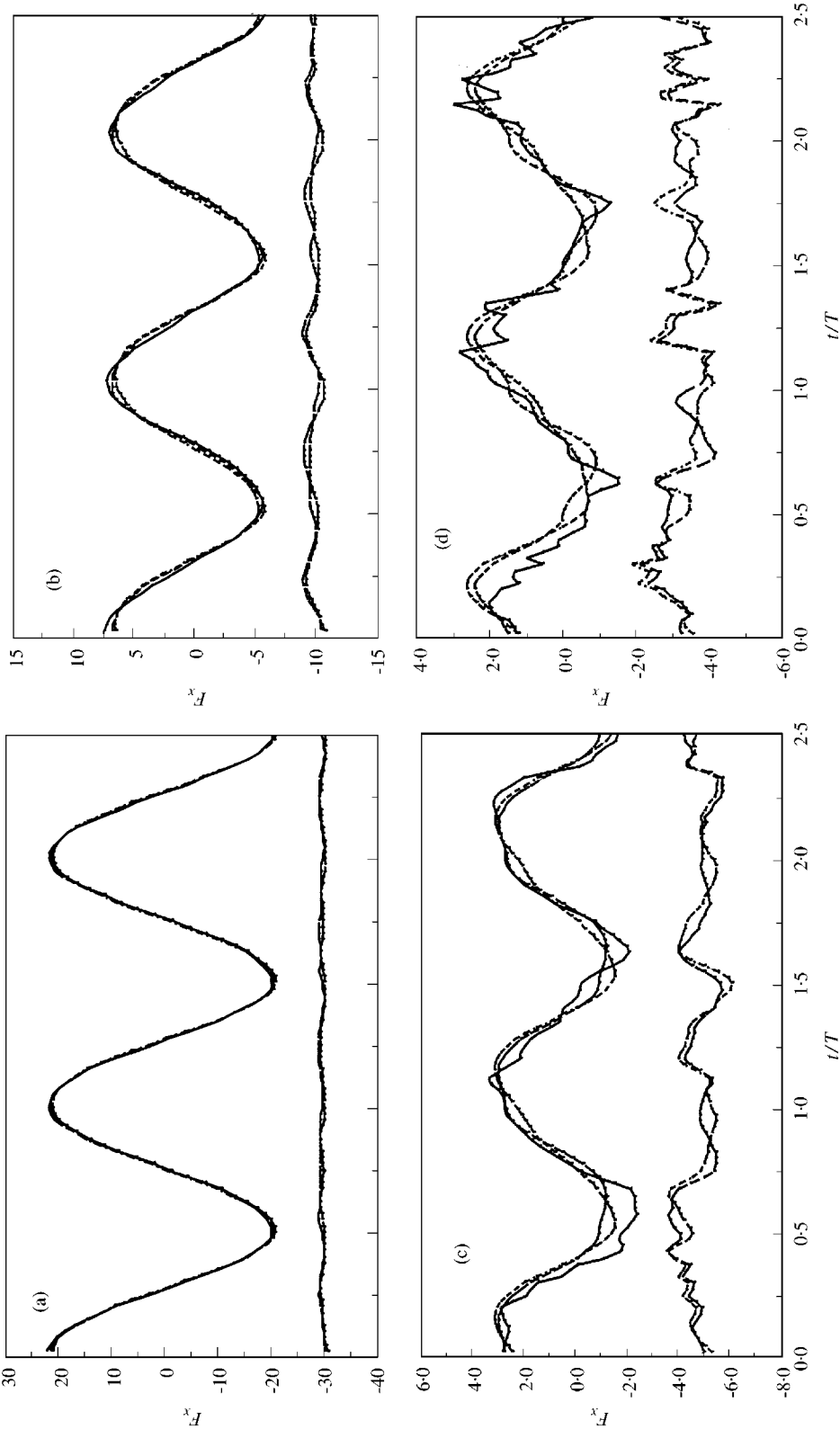

Figure 10. Comparison between reconstructed forces from equations (2) and (3) and computed force: (a) KC = 1, (b) KC = 3, (c) KC = 8, (d) KC = 18; $\beta = 200$. Top curves: – – –, Computer force; –·–·–, equation (2); ---, equation (3). Bottom curves: –·–·–, error, equation (2); – – –, error, equation (3).

TABLE 3

The r.m.s. values of residue of reconstructed forces ΔF_{rms} for $B = 0{\cdot}5$

	Equations	KC = 1	KC = 3	KC = 8	KC = 18	KC = 26
1	Eq. (2) with C_{d1} & C_{d2}	0·063	0·082	0·155	0·122	0·145
2	Eq.(3) with C_{do} & C_{dc}	0·031	0·064	0·124	0·129	0·155
3	Eq.(2) with C_{d1} at $B = 0$	0·097	0·105	0·191	0·181	0·185

force for KC = 1 where the inertia force is the dominant part of the total force. As KC increases and the drag force becomes more important, the divergence of the reconstructed forces from the calculated force becomes larger.

In Figure 10(c–d) the higher frequencies may be seen in the computed force history which come from the vortex shedding. These higher frequency components cannot be simulated by equations (2) and (3) with undisturbed velocity and constant coefficients evaluated from a Fourier average. In general, the force coefficients, assuming that equations (2) and (3) hold exactly at all times through the cycle, vary with time. In the cases shown in Figure 10(c,d), it is conceivable that these force coefficients vary with time very much.

For comparison, ΔF_{rms}, the r.m.s. value of the residue of various reconstructed in-line forces less the actual in-line force (computed), defined as

$$\Delta F_{\text{rms}} = \frac{2}{(F_{x_{\max}} - F_{x_{\min}})} \sqrt{\frac{\sum_{i=1}^{n} (F_{x_i}^{*}(t) - F_{x_i}(t))^2}{n}}, \tag{23}$$

is presented, where $F_{x_i}^{*}(t)$ and $F_{x_i}(t)$ are the reconstructed and actual forces respectively, and $\frac{1}{2}(F_{x_{\max}} - F_{x_{\min}})$ is the amplitude of the computed force. The results for $B = 0{\cdot}5$ at different KC are given in Table 3. It is seen that, for the given value $B = 0{\cdot}5$, equation (3) gives a better force fit than equation (2) when KC ≤ 8, while (2) tends to give a better one when KC ≥ 18 (see rows 1 and 2 in Table 3). Equation (2) with a single drag coefficient value for planar oscillatory flow with no current (i.e. row 3 in Table 3) gives a less accurate force fit than the others. The value of ΔF_{rms} generally increases as KC increases. This is associated with the formation and shedding of more vortices per flow cycle as KC increases and the fact that equations (2) and (3) with the time-averaged coefficients are not able to model the high harmonics generated by the vortex shedding in the moderate KC regime.

7.2. TWO EXTREME CASES

Two extreme cases studied here are as follows: $V_r \gg$ KC, i.e. large B, and KC $\gg V_r$, i.e. small B. For the first extreme it has been found that there is no significant coupling between the small-amplitude oscillations and the vortex shedding. The drag coefficient associated with the mean flow would essentially remain constant at its steady-state value, at least for the velocity ratio B larger than about 7 (Sarpkaya & Isaacson 1981). For the second extreme, Verley & Moe (1979b) suggested that one may tentatively conclude that for high waves (oscillatory flow) plus a small current (i.e. small B), the modified Morison's equation (2) may be used with some confidence using values of C_d and C_m obtained under pure wave (planar oscillatory motion). An investigation for these two cases, with $B = 10$ and Re = 200 and with $B \leq 0{\cdot}1$ and KC = 4, is carried out in this section.

The result for the first extreme, i.e. combination flow with $B = 10$ and Re = 200, shows that the r.m.s. value of the residue between computed force and the reconstructed force

TABLE 4

The r.m.s. values of residue of reconstructed forces for KC = 4

Equation	$B = 0{\cdot}05$	$B = 0{\cdot}1$	$B = 0{\cdot}15$	$B = 0{\cdot}25$
Equation (2)	0·051	0·057	0·070	0·074

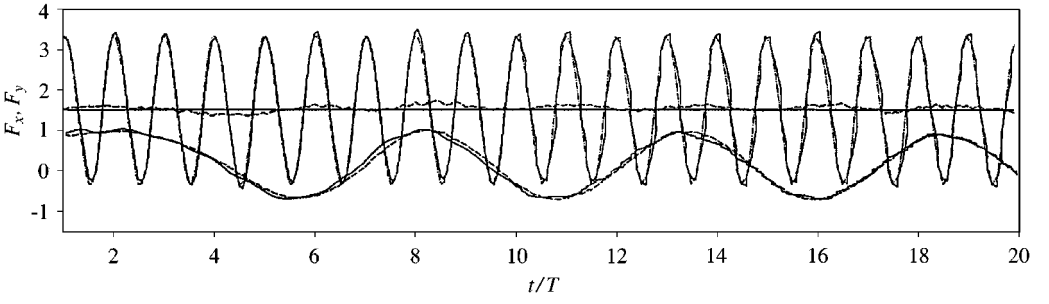

Figure 11. In-line and lift forces on a circular cylinder in combined flow with Re = 200 and $B = 10$: ——, calculated force for the combination flow; ----, calculated force for steady flow of Re = 200; -·-·-, reconstruction force using equation (2) with C_d value of steady flow.

using equation (2) with a value of C_d taken from the steady current case is very similar to that using equations (2) with C_{d1} and C_{d2} (only 1·3% difference). The results of force histories are plotted in Figure 11. It is seen that the mean value of the in-line force and the lift force are very close to the values for the steady current and the reconstructed force by using the value obtained for the steady current case at this velocity ratio gives a good fit to the computed force.

For the other extreme case, i.e. very small B, the r.m.s. values of residue of the reconstructed force using equation (2) with C_d and C_m v alue of planar oscillation flow are illustrated in the Table 4, where KC = 4 and a variable B.

As shown in the table, the r.m.s. values of the residue between the reconstructed force and the computed force are less than 10% which suggests that, when $B < 0{\cdot}25$, use of equation (2) with C_d and C_m values obtained from planar oscillatory flow can give reasonably good in-line forces fit for the combination flow.

8. DISCUSSION ON VORTEX PATTERNS

It is known that there is a general relationship between KC and the onset of flow separation, symmetrical and asymmetrical vortices for planar oscillatory flow as has been described earlier. It is attempted in this section to examine this relationship when there is a current. The vortex patterns presented here are for $B = 1$.

8.1. ONSET AND SHEDDING OF VORTEX WAKES

At small oscillation KC (small enough to give attached flow when there is no current) with a very small current so that Re ≤ 47, there is no separation. The force exerted by fluid motion on the cylinder is dominated by the oscillations and the oscillatory drag and inertia coefficients are hardly affected by the small current.

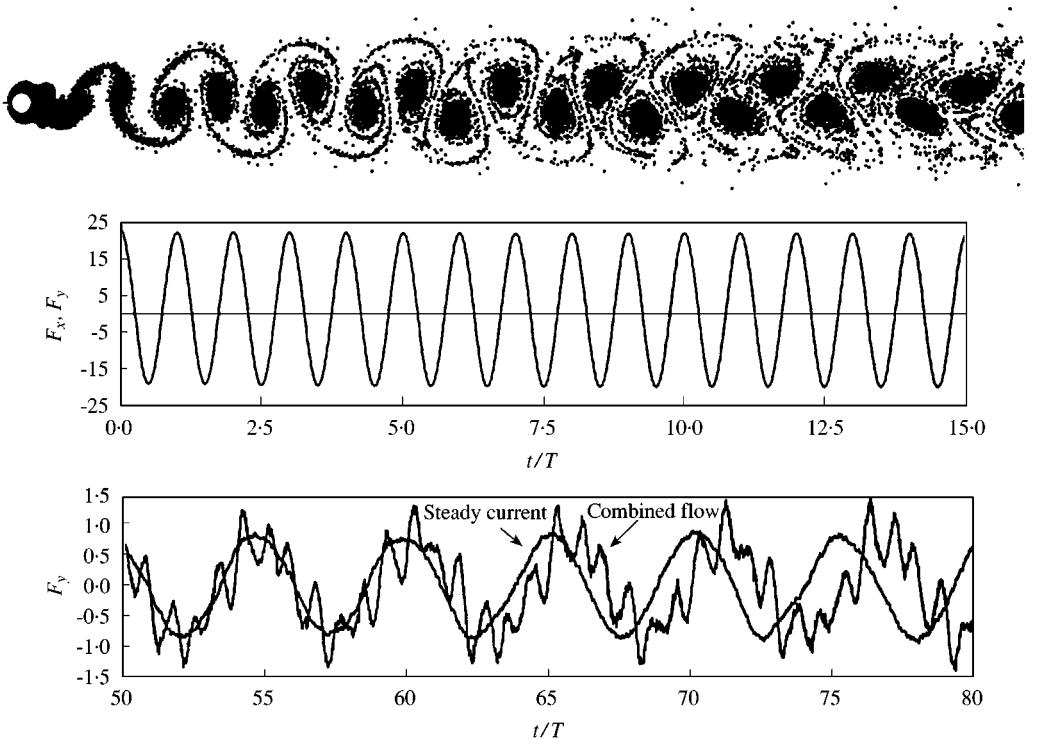

Figure 12. (a) Vortex pattern in the wake for combined flow with KC = 1·0 and Re = 200 ($B = 1$); (b) force time histories for combined flow with KC = 1·0 and Re = 200; (c) lift force time histories of a combined flow with KC = 1·0 and Re = 200 and a steady current with Re = 200.

At slightly larger amplitude of oscillation, small KC plus slightly larger current such that Re $\sim$ 100 (to keep $B = 1$), the Karman vortex street, which occurs due to the current alone at Re = 100, is retained [see Figure 9(a)]. The period taken by a vortex to form and shed from one side of the cylinder is more than six times the period of the oscillations.

As KC increases up to 1 and Re increases to 200 (keeping $B = 1$), one large vortex forms in the near wake and is shed respectively from each side of the near wake to form a Karman vortex street [see Figure 12(a)]. The amplitude of the lift force coefficient is seen to be increased to about twice as large, compared to that for a steady current alone [see Figure 12(c)].

8.2. Symmetric Shedding—A Pair of Symmetric Vortices Per Cycle

As KC increases up to 2 and Re to 400, one pair of symmetric vortices is shed each cycle. One pair of vortices with opposite sign starts to form behind the cylinder as the oscillatory motion moves with the current. When the oscillatory motion moves against the current, they move towards the cylinder and another pair of small vortices forms and grows. As the oscillation motion starts to move with the current again, the new pair of vortices symmetrically grows, rolls up and moves away from the cylinder on each side, while the previous pair of vortices spreads out [see Figure 13(a)]. Simultaneously, another pair of vortices, similar to the first pair of vortices, forms behind the cylinder. In each cycle, two pairs of symmetrical vortices form. The second pair is shed, while the first pair spreads out. As the oscillatory motion continues to move with and against the current, a series of pairs of vortices

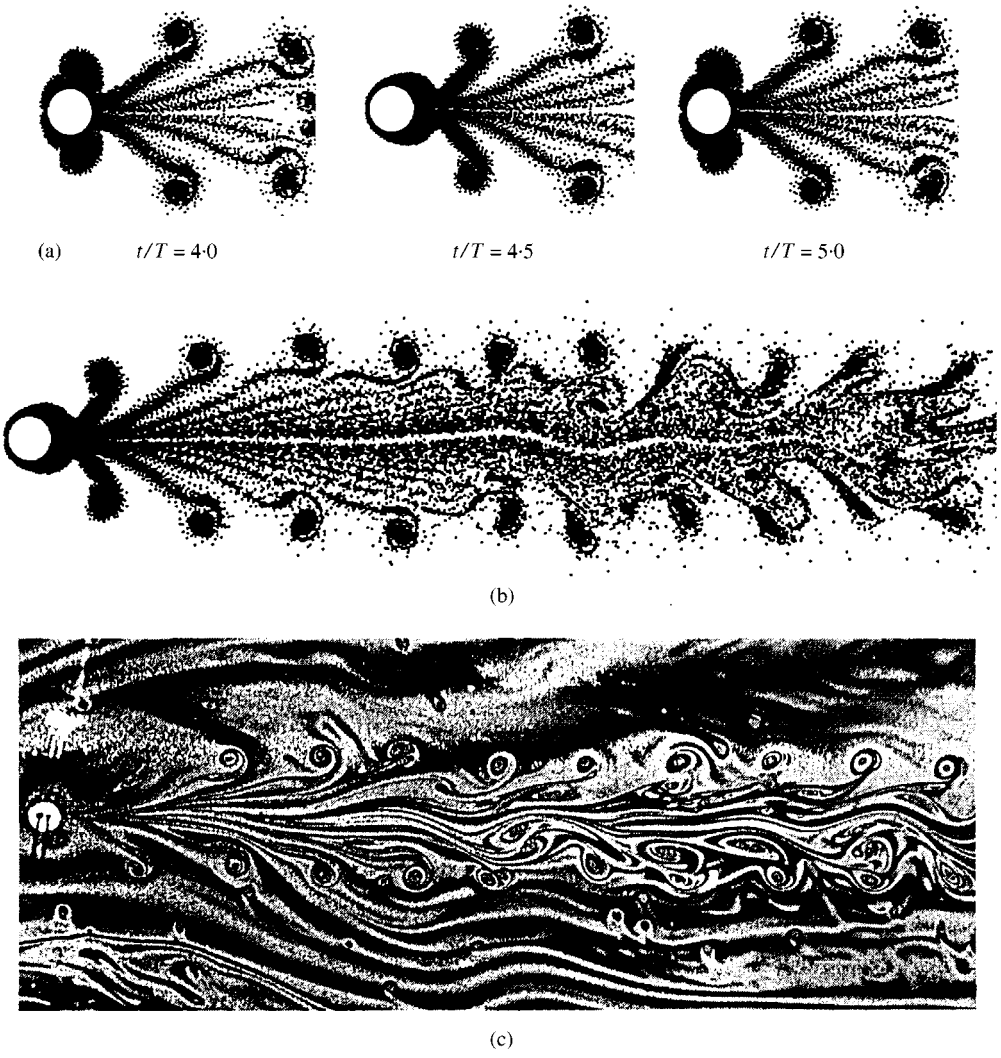

Figure 13. (a) Symmetric vortex shedding — a pair of symmetric vortices per cycle of combined flow with KC = 2 and Re = 400 ($B = 1$). (b,c) Comparison of vortex pattern in the wake: (b) present computational results and (c) experimental visualization by Couder & Basdevant (1986).

shed from the cylinder and move away downstream. The vortex pattern in the wake [Figure 13(b)] is seen to be similar to an analogous experiment visualized by Couder and Basdevant (1986) [see Figure 13(c)] using soap film which exhibits two-dimensional vortex shedding, where the cylinder is oscillating in the fluid with the same frequency of the symmetric vortex shedding.

8.3. Symmetric Shedding—A Pair Of Symmetric Vortex Pairs Per Cycle

As KC increases up to 3·0 and Re to 600 (to keep $B = 1$), the process of forming, growing and shedding of vortices is very similar to the one described above, but the second pair of vortices forms earlier, and the first pair of the vortices does not spread out but combines with the second pair as a pair of symmetrical couples [two vortices of opposite sign, see Figure 14(a)]. At each cycle, one pair of symmetrical vortex pairs forms, grows and sheds. As the oscillatory motion moves with and against the current, a series of double vortex pairs are generated and form a nearly symmetrical pattern in the near wake [see Figure 14(b)]. However, this wake is very unstable and soon starts to reorganize itself to form a Karman-type alternating vortex wake. Similar phenomena are also seen for the flow with $KC = 2$ and $Re = 400$ in the far wake. This process is associated with the instability of the symmetric vortex wake and the greater stability of a Karman-type alternating vortex wake. This latter is formed rather further downstream than would occur for a cylinder in a current alone.

Verley & Moe (1979b) also found from their experiments that the wake changes from a symmetric to an alternating wake commencing downstream in the wake and then working its way up to the cylinder with the wake remaining symmetric for a distance downstream of typically three to five diameters for low B values.

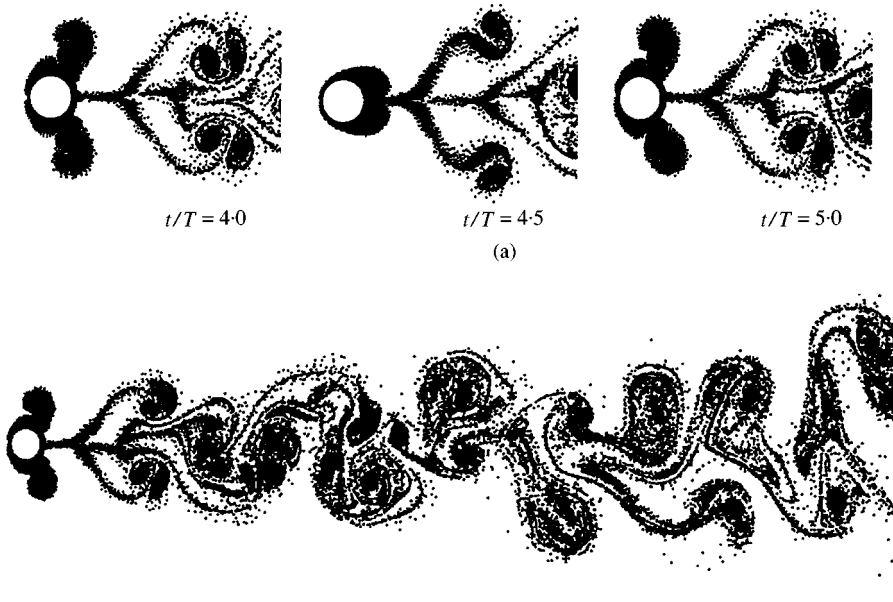

Figure 14. Symmetric vortex shedding — a pair of symmetric couples per cycle, at different t/T; combined flow with $KC = 3$ and $B = 1$.

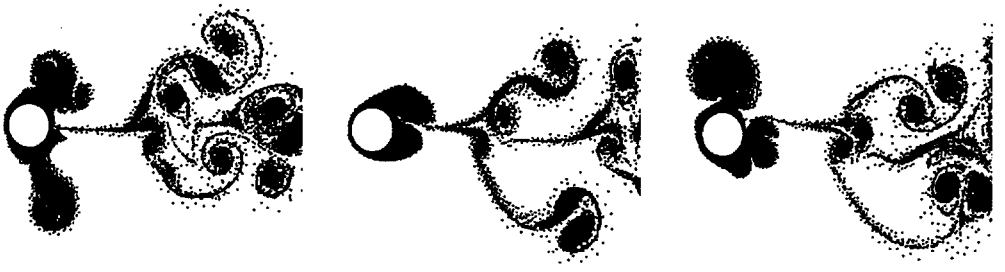

Figure 15. Asymmetric shedding — a pair of asymmetric couples per cycle, at different t/T; combined flow with KC = 4 and $B = 1$.

8.4. Asymmetric Shedding—A Pair Of Asymmetric Couples Per Cycle

As KC increases further up to 4 (keeping $B = 1$), the influence of the asymmetrical wake makes its way right up to the cylinder, immediately after two symmetrical pairs of vortex couples have been shed in the first two cycles. A pair of asymmetrical eddies forms in the first half of the fourth cycle and is then shed asymmetrically as two associated vortex pairs with the second pair of vortices, growing in the second half of the cycle. One pair of the growing vortices appears to be larger than the other [see Figure 15(b)]. In the fifth cycle, the same procedure is repeated but the pairs formed on the other side appears to be the larger, and the pattern in this cycle is the mirror image of that in the fourth cycle (Figure 15).

9. CONCLUSIONS

An investigation on combined motion of an oscillatory flow plus a current past a circular cylinder has been carried out. These flows are computed for Keulegan–Carpenter numbers in the range 0·2–26 and with the Stokes parameter set at 200. A vortex-based method incorporating Lagrangian vortex particles with an Eulerian, mesh-based, finite-difference scheme for the velocity field and viscous diffusion is used. The effects of small current on force coefficients and vortex shedding and vortex pattern in the wake are examined. An extended Morison's equation and an equation with two drag coefficients are examined and comparisons between these two equations are made.

It is found that the effect of current is to reduce the drag coefficient for the case covered in the present study. This is in agreement with some previous experiments. The current, if it is large enough, causes the flow to separate in the low KC regime, even though the drag coefficients from the oscillatory component of the in-line force behave nearly identically as for planar oscillatory Stokes flow in this regime.

The results of analysing the residues between reconstructed force, using the extended Morison's equation (2) and the basic simulated force data and for the equation with two drag terms (3), suggest that the former gives a better force fit for the higher KC range ($KC \geq 18$), while the latter does so for the lower range ($KC \leq 8$). It is found that, when $B < 0{\cdot}25$, i.e. very small current, use of the extended Morison's equation (2) with C_d and C_m values obtained from planar oscillatory flow can give reasonably good in-line forces fit for the combination flow cases covered in the present study.

In the presence of significant current, symmetric vortex shedding and asymmetrical vortex shedding are found at low values of KC. In the symmetric vortex-shedding case, the symmetrical pattern of the wake persists a distance downstream from the cylinder and then

becomes unstable and asymmetrical. The asymmetric influence makes its way up to the cylinder as KC increases. When KC increases up to a critical value, e.g. KC = 6 for $B = 1$, this effect reaches the back of the cylinder and changes the vortex shedding itself from symmetric to an asymmetric pattern. Hence, the wake always tries to form a Karman type of vortex street, irrespective of how the vortices are shed from the cylinder. The phenomena predicted by the numerical simulation of vortex formation, shedding and vortices moved backward and forward by oscillatory flow in the current are similar to effects observed in some previous experiments.

Finally, this study has shown that the vortex method used in the present work gives good representations for steady flow, oscillatory flow and also for the combination of the two flows for the force coefficients, Strouhal numbers and vortex patterns in the wake.

ACKNOWLEDGEMENTS

C.Y. Zhou is grateful to the U. K. Science and Engineering Research Council for the support given to her for her Ph.D. studies in Imperial College.

References

Bearman, P. W. 1998 Developments in the understanding of bluff body flows. *JSME International Journal*; *Series B*, *Fluids and Thermal Engineering* **41,** 103–109.

Bearman, P. W., Downie, M. J., Graham, J. M. R. & Obasaju, E. D. 1985 Forces on cylinders in viscous oscillatory flow at Keulegan-Carpenter numbers. *Journal of Fluid Mechanics* **154,** 337–356.

Bearman, P. W., Graham, J. M. R. & Singh, S. 1978 Forces on cylinders in harmonically oscillating flow. Presented at the *IAHR Symposium on Mechanics of Wave-induced Forces on Cylinders*, University of Bristol, September.

Chaplin, J. R., Graham, J. M. R., Stansby, P. K. & Younis, B. A. 1992 Benchmarking of CFD codes for fluid loading applications. Report, City University, London, U.K.

Chorin, A. J. 1973 Numerical study of slightly viscous flow. *Journal of Fluid Mechanics* **57,** 785–796.

Christiansen, J. P. 1973 Numerical simulation of hydrodynamics by the method of point vortices. *Journal of Computational Physics* **13,** 363–379.

Couder, Y. & Basdevant, C. 1986 Experimental and numerical study of vortex couples in two-dimensional flows. *Journal of Fluid Mechanics* **173,** 225–251.

Dalrymple, R. A. 1975 Waves and wave forces in the presence of currents. *Proceedings Civil Engineering in the Oceans III*, *ASCE*, University of Delaware, pp. 999–1018.

Graham, J. M. R. 1988 Computation of viscous separated flow using a particle method. In *Numerical Methods in Fluid Mechanics* (ed. K. W. Morton). Vol. 3, pp. 310–317. Oxford: Oxford University Press.

Honji, H. 1981 Streaked flow around an oscillating circular cylinder. *Journal of Fluid Mechanics* **107,** 509–520.

Justesen, P. 1991 A numerical study of oscillating flow around a circular cylinder. *Journal of Fluid Mechanics* **222,** 157–196.

Keulegan, G. H. & Carpenter, L. H. 1958 Forces on cylinders and plates in an oscillating fluid. *Journal Research of the National Bureau of Standards* **60,** 423–440.

Koumoutsakos, P., Leonard, A. & Pepin, F. 1994 Boundary conditions for viscous vortex methods. *Journal of Computational Physics* **113,** 52–61.

Lin, X. W., Bearman, P. W. & Graham, J. M. R. 1996 A numerical study of oscillatory flow about a circular cylinder for low values of beta parameter. *Journal of Fluids and Structures* **10,** 501–526.

Morison, J. R., O'brien, M. P., Johnson, J. W. & Schaaf, S. A. 1950 The force exerted by surface waves on piles. *AIME Petroleum Transactions* **189,** 149–157.

Obasaju, E. D., Bearman, P. W. & Graham, J. M. R. 1988 A study of forces, circulation and vortex patterns around a circular cylinder in oscillating flow. *Journal of Fluid Mechanics* **196,** 467–494.

Obasaju, E. D., Bearman, P. W. & Graham, J. M. R. 1991 In-line forces on a cylinder performing large amplitude oscillation in a steady current. *Proceedings* 1*st International Offshore and Polar Engineering Conference*, Edinburgh, pp. 340–345.

Sarpkaya, T. 1986 Force on a circular cylinder in viscous oscillatory flow at low Keulegan–Carpenter numbers. *Journal of Fluid Mechanics* **165,** 61–71.

Sarpkaya, T. & Isaacson, M. 1981 *Mechanics of Wave Forces on Offshore Structures*. New York: Van Nostrand Reinhold.

Sarpkaya, T., C. Putzig, D. Gordon, X. WANG & C. Dalton 1992 Vortex trajectories around a circular cylinder in oscillatory plus mean flow. *Journal of Offshore Mechanics and Arctic Engineering* **114,** 291–298.

Sarpkaya, T. & Storm, M. 1985 In-line force on a cylinder translating in oscillatory flow. *Applied Ocean Research* **7,** 188–195.

Verley, R. L. P. & Moe, G. 1979a The effect of cylinder vibration on the drag force and the resultant hydrodynamic damping. *Mechanics of Wave-Induced Forces on Cylinders* (ed. T. L. Shaw), pp. 521–531. London: Pitman.

Verley, R. L. P. & Moe, G. 1979b The forces on a circular cylinder oscillating in current. River and Harbour Laboratory, The Norwegian Institute of Technology Report No. STF60 A79061.

Wang, C. Y. 1968 On high-frequency oscillatory viscous flows. *Journal of Fluid Mechanics* **32,** 55–68.

Williamson, C. H. K. 1985 Sinusoidal flow relative to circular cylinders. *Journal of Fluid Mechanics* **155,** 141–174.

Wu, J. L. 1981 Theory for aerodynamic force and moment in viscous flows. *AIAA Journal* **19,** 432–449.

Zhou, C. Y. 1994 Effects of combination motion on cylinders in waves and currents. Ph.D. Thesis, Imperial College, University of London, U.K.